Compressible turbulent channel flow with impedance boundary conditions

By C. Scalo, J. Bodart†, S. K. Lele AND L. Joly†

We have performed a total of 30 wall-resolved large-eddy simulations (LES) of isothermal-wall compressible turbulent channel flow at a bulk Reynolds number $\mathrm{Re}_b = 6900$ and Mach numbers $\mathrm{M}_b = 0.05, 0.2, 0.5$. Linear acoustic impedance (IBCs) and no-slip boundary conditions were used for the wall-normal and tangential velocity components, respectively. The IBCs are formulated in the time domain following Fung & Ju (2004) and coupled with a fully explicit compressible Navier-Stokes solver, preserving spatial and temporal consistency of the discretization. The impedance model adopted is a three-parameter damped Helmholtz oscillator with undamped angular frequency, ω_r, tuned to the characteristic time scale of the outer layer large eddies. Normalizing with the speed of sound and channel semi-height, the tuning condition becomes $\omega_r = 2\pi \mathrm{M}_b$. This reduces the degrees of freedom of the IBCs to two: the damping ratio, ζ, and the resistance, R, which have been investigated in the range, $\zeta = 0.5, 0.7, 0.9$, and $R = 0.01, 0.10, 1.00$. For each M_b a reference case with isothermal walls has also been performed. The application of the tuned IBCs results in a noticeable drag increase for sufficiently high M_b and/or low R, exceeding 300% for $\mathrm{M}_b = 0.5$ and $R = 0.01$, and thus represents a promising passive control technique for delaying boundary-layer separation and/or enhancing wall heat transfer. No significant differences in the flow response are observed by varying the damping ratio in the range investigated. Alterations to the turbulent flow structure are confined to approximately the first 15% of the boundary-layer thickness where buffer-layer coherent vortical structures are entirely replaced by an array of spanwise Kelvin-Helmholtz-like rollers. The Reynolds shear stress gradient at the wall becomes non-zero, resulting in the disappearance of the viscous sublayer and departure of the mean velocity from the law of the wall. The computational domain size and resolution have a neglibile effect on first and second-order statistics, confirming the quality of the exploratory set of LES.

1. Introduction

In low-speed boundary layers acoustic perturbations are evanescent wave modes. As compressibility effects become more important, wave energy can amount to a sensible portion of the overall fluctuating energy with the potential to actively affect the flow dynamics. In this work we explore the possibility of altering the structure of a compressible turbulent boundary layer by controlling the reflection of waves at the wall. This can be achieved by introducing a linear acoustic element modeled by the impedance boundary condition

$$\hat{p} = Z(\omega)\hat{v} \tag{1.1}$$

where $\hat{p}$ and $\hat{v}$ are the complex pressure and velocity amplitudes, and $Z(\omega)$ is the acoustic impedance. The wall-normal velocity $\hat{v}$ in the Eq. (1.1) is positive if directed away from

† Université de Toulouse, ISAE, France

the fluid side. In the present paper, all quantities are made dimensionless with a reference density, speed of sound and length scale. The time harmonic behavior $e^{+i\omega t}$ is assumed where ω is the angular frequency.

For the purposes of the present work we have coupled a single damped Helmholtz oscillator, represented by the three-parameter broadband impedance (2.9) with a compressible turbulent channel flow. Similar studies have looked at the interaction of a supersonic compressible boundary layer with a fluttering panel (Ostoich *et al.* 2013) and a high-speed grazing flow interacting with two-dimensional liners (Zhang & Bodony 2012). Direct approaches in similar contexts, such as the one in Tam *et al.* (2013), have investigated a grazing flow in an impedance tube with a developing laminar boundary layer resolving the resonator geometry and have observed a drag increase, consistently with our results. Bres *et al.* (2013) investigated the stability properties of a two-dimensional hypersonic boundary layer over absorptive coatings by resolving the pore geometry and derived a simple impedance model for companion linear stability calculations.

Analogous studies in the incompressible regime have investigated near-wall turbulence interacting with a porous wall (Jiménez *et al.* 2001) modeled by Darcy-type boundary conditions. These resulted in a large friction drag increase as well as structural changes to the near-wall turbulent motions. Spanwise-coherent rollers accounted for the wall-friction increase and near-wall velocity streaks were weakened and enhanced, respectively, in suction and blowing regions, both exhibiting extended spanwise coherence. The increase in wall friction thus did not result from the strengthening of the classical wall-turbulence cycle (Jiménez & Pinelli 1999). Very similar flow response dynamics are observed in the context of the present numerical simulations, where near-wall streaks are completely removed by the application of tuned IBCs.

Although a comprehensive overview of the structure of a turbulent compressible boundary layer with flat, isothermal walls can be found in the works by Huang *et al.* (1995), Coleman *et al.* (1995), Lechner *et al.* (2001), Foysi *et al.* (2004), and Ghosh *et al.* (2010), to our knowledge, no previous study has explored the interaction of IBCs with near-wall compressible turbulence and/or outlined the details of the coupling between time-domain impedance boundary conditions (TDIBC) and a fully compressible Navier-Stokes solver. The simplicity and uniqueness of the proposed setup has motivated the present study.

The governing equations and boundary conditions are analyzed to identify the proper set of dimensionless numbers, resulting in the definition of a parameter space with three degrees of freedom: the bulk Mach number, M_b, the IBC's damping ratio, ζ, and resistance, R. Other dimensionless parameters such as the Prandtl number, Pr, and the Reynolds number based on the speed of sound Re_a and bulk velocity Re_b and the IBC's undamped resonant frequency are either set as constants or depend on the set M_b, ζ, R. Baseline results for a turbulent compressible channel flow are reproduced with IBCs acting as hard walls (i.e. in the limit of $|Z(\omega)| \to \infty$) and are validated against other numerical simulations available in the literature for isothermal walls. Finally, results from turbulent channel flow coupled with impedance boundary conditions, exploring the aforementioned parameter space, are analyzed and discussed.

2. Problem Formulation

2.1. *Governing equations*

In this section we present the complete set of governing equations and boundary conditions to determine the appropriate dimensionless parameter space to explore. Hereafter,

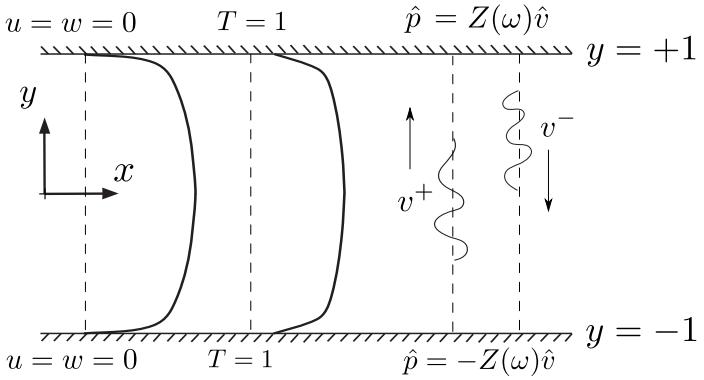

FIGURE 1. Sketch showing impedance boundary conditions interacting with wall-normal waves in a compressible turbulent channel flow. All quantities shown are non-dimensionalized with the speed of sound based on the wall temperature and the channel half-width. The negative sign for the lower-wall impedance condition is necessary to preserve symmetry (see velocity convention in Eq. (1.1)).

all reported quantities are non-dimensionalized with the speed of sound based on the wall temperature, the channel half-width, and bulk density (constant for channel-flow simulations). The governing equations are

$$\frac{\partial}{\partial t}\rho + \frac{\partial}{\partial x_j}\left(\rho u_j\right) = 0 \tag{2.1}$$

$$\frac{\partial}{\partial t}\left(\rho u_i\right) + \frac{\partial}{\partial x_j}\left(\rho u_i u_j\right) = -\frac{\partial}{\partial x_i}p + \frac{1}{\mathrm{Re}}\frac{\partial}{\partial x_i}\tau_{ij} + f_1(\mathrm{M}_b)\,\delta_{1i}, \tag{2.2}$$

$$\begin{aligned}\frac{\partial}{\partial t}\left(\rho T\right) + \frac{\partial}{\partial x_i}\left(\rho u_i T\right) = (\gamma-1)\left[\frac{\partial p}{\partial t} + u_i\frac{\partial p}{\partial x_i}\right] + \\ + \frac{1}{\mathrm{Re}\,\mathrm{Pr}}\frac{\partial}{\partial x_j}Q_j + \frac{\gamma-1}{\mathrm{Re}}\tau_{ij}\frac{\partial u_i}{\partial x_j},\end{aligned} \tag{2.3}$$

where the gas is ideal with equation of state $p = \gamma^{-1}\rho T$, and Re and Pr are the Reynolds number and Prandtl numbers based on the reference viscosity, and γ is the ratio of specific heats. The normalized viscous and conductive heat fluxes are

$$\tau_{ij} = 2\mu\left[S_{ij} - \frac{1}{3}\frac{\partial u_m}{\partial x_m}\delta_{ij}\right], \tag{2.4}$$

$$Q_j = -\mu\frac{\partial T}{\partial x_j} \tag{2.5}$$

where S_{ij} is the strain-rate tensor and μ the dynamic viscosity, respectively given by $S_{ij} = (1/2)\left(\partial u_j/\partial x_i + \partial u_i/\partial x_j\right)$, and $\mu = T^n$ where n is the viscosity exponent. The dynamic viscosity is normalized with its value at the wall temperature, which corresponds to the reference value used in Re and Pr. The body force f_1 in Eq. 2.1(b) is applied only in the streamwise direction and dynamically adjusted to achieve the desired bulk Mach number, $\mathrm{M}_b = \langle\rho\,u\rangle_{\mathcal{V}}/\langle\rho\rangle_{\mathcal{V}}$, where $\langle\cdot\rangle_{\mathcal{V}}$ is the volume-averaged operator.

The IBCs, no-slip conditions for the tangential velocities and the isothermal conditions

$$\hat{p} = \pm Z(\omega)\,\hat{v} \tag{2.6}$$

$$u = w = 0 \tag{2.7}$$

$$T = 1, \tag{2.8}$$

respectively, are applied at the walls, $y = \pm 1$, and the impedance $Z(\omega)$ is given by

$$Z(\omega) = R + i\left[\omega\, X_{+1} - \omega^{-1} X_{-1}\right], \tag{2.9}$$

where R is the resistance and X_{+1} and X_{-1} are the acoustic mass and stiffness, respectively, and ω is the angular frequency. For a given value of the resistance, R, the acoustic mass, X_{+1}, and stiffness, X_{-1}, can be expressed as a function of undamped resonant angular frequency, ω_r, and damping ratio, ζ, where

$$\omega_r = \sqrt{X_{-1}/X_{+1}} \tag{2.10}$$

$$\zeta = \frac{1+R}{2\,\omega_r\, X_{+1}}. \tag{2.11}$$

Damping ratios higher than 1 lead to inadmissible (or anti-causal) impedance and, therefore, will not be considered. For a given value of the resistance R, fixing ω_r and ζ in (2.10) is equivalent to fixing the dimensionless acoustic mass and stiffness in (2.9) and vice versa. By chosing $\mathrm{Pr} = 0.72$, $n = 0.76$ (Shang & Wang 1990) and $\gamma = 1.4$ only five dimensionless parameters are left: two in the governing flow equations, Re and M_b, and three in the wall impedance, R, X_{+1}, and X_{-1}, or, alternatively, R, ζ, and ω_r. The Reynolds number based on the bulk velocity is given by $\mathrm{Re}_b = \mathrm{Re}\,\mathrm{M}_b$.

2.2. *Computational setup*

For the scope of the present study the aforementioned parameter space had to be reduced. For all cases investigated the bulk Reynolds number is fixed to $\mathrm{Re}_b = 6900$ in order to obtain a well-developed turbulent flow while maintaining the computational effort manageable. Preliminary numerical trials have shown that tuning of the normalized IBC's undamped resonant angular frequency, ω_r, to the characteristic time scale of the outer scale eddies,

$$\omega_r = 2\pi \mathrm{M}_b, \tag{2.12}$$

results in a noticeable drag increase. The constant flow rate calculations allow such tuning condition to be enforced with a constant value for ω_r.

While a more systematic analysis on the effects of varying ω_r is deferred to future studies, preliminary numerical investigations show that choosing ω_r to be one order of magnitude larger or smaller than the tuning condition in Eq. (2.12), yields to a negligible alteration of the flow (detuned IBCs). On the other hand, a very similar response to the one observed in the present manuscript was obtained by choosing $\omega_r = 2\pi \mathrm{M}_\infty$ where M_∞ is based on the centerline velocity (instead of bulk velocity), showing the robustness of the tuning.

By imposing Eq. (2.12) for all cases, the parameter space is finally reduced to the bulk Mach number, M_b, the damping ratio, ζ, and the resistance, R. A set of three values for each parameter has been explored resulting in a total of 27 large-eddy simulations (LES) for all combinations of $\mathrm{M}_b = \{0.05, 0.2, 0.5\}$, $\zeta = \{0.5, 0.7, 0.9\}$, and $R = \{0.01, 0.10, 1.00\}$. The chosen values for the resistance bracket the value of 0.18 obtained in Tam & Auriault (1996) by calibrating Eq. (2.9) against the response of a realistic perforated

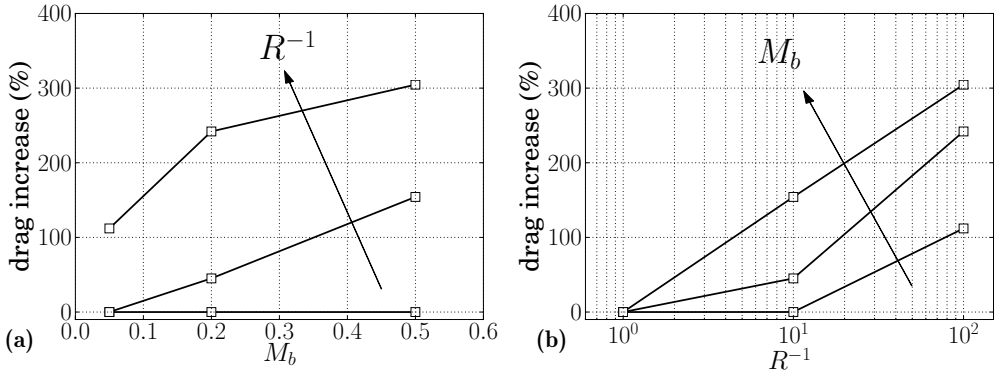

FIGURE 2. Drag increase (%) with respect to a baseline case, obtained separately for each M_b without IBCs, averaged over all values of ζ. (a) Drag increase versus bulk Mach number for different values of R^{-1} and (b) versus R^{-1} for different values of M_b . In all cases, the undamped angular frequency, ω_r, has been tuned to the large scales according to Eq. (2.12).

panel. Three additional LES with simple isothermal walls have also been performed for each Mach number to serve as reference cases.

All of the aforementioned exploratory LES are run with respective streamwise, wall-normal and spanwise grid resolutions of $\Delta x^+ < 40$, $\Delta y^+_{\rm min} < 0.7$ and $\Delta z^+ < 15$, and with the Vreman (2004) sub-grid scale model active. The computational domain size has been chosen to properly accommodate the near-wall and outer layer turbulent structures in the low-Mach-number limit. A sensitivity study of the grid resolution and domain size has been carried out for the $M_b = 0.5$ and $R = 0.01$ case (not shown), which, as discussed in the following, exhibits the strongest response.

The governing equations are solved for mass, momentum, and total energy in the finite-volume unstructured code CharLES^x developed as a joint-effort project among researchers at Stanford University. The flux reconstruction method is grid-adaptive at the preprocessing stage and solution-adaptive at run-time. It blends a high-order polynomial interpolation scheme (up to fourth-order accurate on uniform meshes) with a lower-order scheme to ensure numerical stability in areas of low-grid quality (Ham *et al.* 2007). The discretized system of equations is integrated in time with a fully-explicit, third-order Runge-Kutta scheme.

3. Results

The tuning of the IBCs in Eq.(2.9) to the characteristic time scale of outer layer eddies Eq. (2.12) leads to a noticeable drag increase in the majority of cases investigated (Figure 2). The IBCs with the largest value of resistance, $R = 1.0$, allow very limited transpiration at the boundary (acting almost as hard walls), leaving the flow structure, hence the drag, unaffected. Bearing in mind the theoretical nature of the present numerical investigation, the results indicate that, for any given M_b, a sufficiently high value of R^{-1} (i.e., a sufficiently high value of surface porosity) can be found, at which the structure of a turbulent boundary layer is altered. The same behavior was observed by Garcia-Mayoral & Jiménez (2011) in their investigation of low-speed boundary layers over riblets.

As the Mach number increases, the onset of drag increase occurs for lower values of R^{-1} (i.e., for less porous walls). For the highest Mach number investigated and lowest

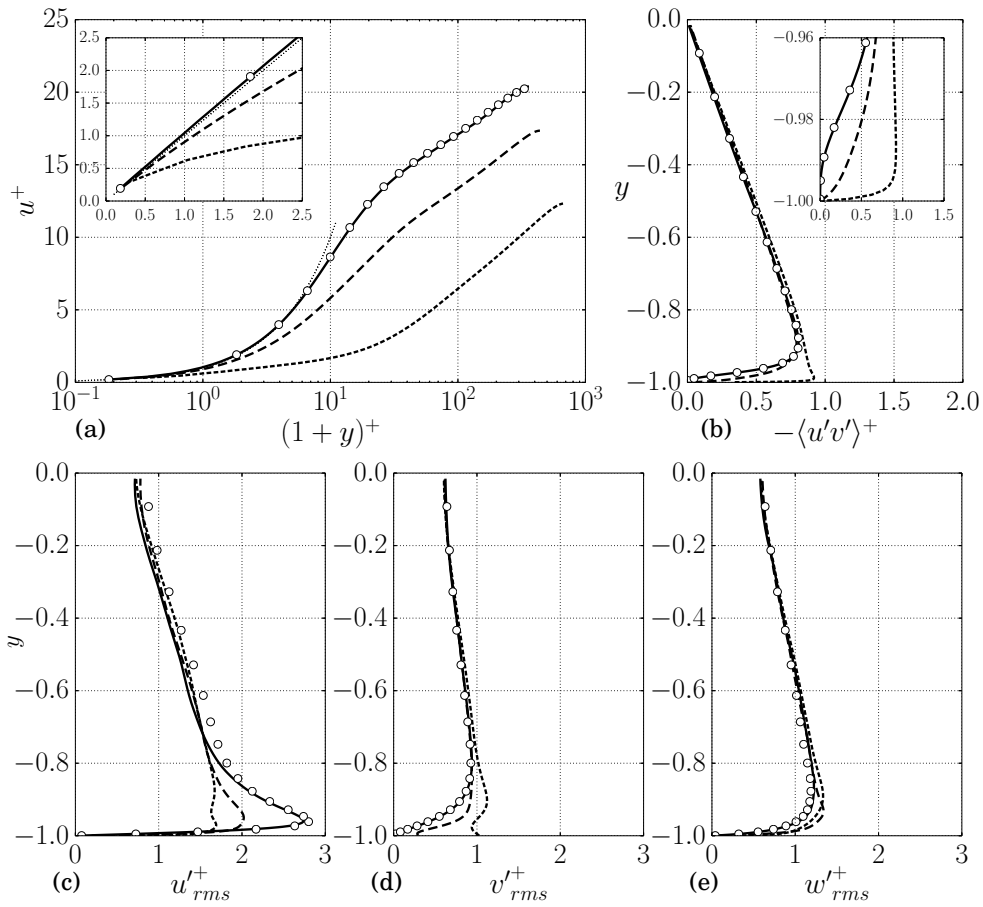

FIGURE 3. (a) Profiles of mean streamwise velocity, (b) resolved Reynolds shear stress and (c) streamwise, (d) wall-normal, and (e) spanwise velocity RMS for $M_b = 0.2$ and $\zeta = 0.5$. Hard-wall case without IBCs (∘) plotted every 8 points, $R = 1.00$ (—), 0.10 (– –) and 0.01 (- - -). (a) Law of the wall $u^+ = (1+y)^+$ ($\cdots$).

value of resistance, the drag increase exceeds 300%. No significant differences in the flow response are observed by varying the damping ratio in the range investigated, apart from a slight increase in the drag as ζ is increased. Unless otherwise specified, the following analysis, for the sake of simplicity, will only focus on the $\zeta = 0.5$ case.

3.1. *Mean profiles and Reynolds stresses*

The observed drag increase is associated with a structural change in the state of near-wall turbulence (Figure 3), which is confined to the region $y < -0.8$. All cases for $R < 1$ show noticeable deviations from the smooth-wall log law (retaining, however, the same Kármán constant) and law of the wall, the latter owing to the non-zero limiting behavior of the Reynolds shear stress gradient at the wall (Figure 3(b),inset). As the resistance is decreased, the near-wall streamwise velocity RMS peak disappears, while the wall-normal velocity variance increases more rapidly than the friction velocity (Figure 3(d)). The latter is associated with the increased permeability at the wall extending the Reynolds shear stress peak very close to the boundary, causing a dramatic thinning of the

viscous sublayer, and, hence, increased drag. As discussed in the following, turbulence production mechanisms are profoundly reshaped by the application of tuned IBCs.

3.2. *Alteration of near-wall turbulent structures*

Two-point autocorrelations (Figure 4) confirm that alterations to the turbulent structure due to the IBCs are confined near the boundary and that no difference is observed between the baseline simulations (without IBC) and the ones with IBCs for high resistances ($R = 1.00$). In the latter case the IBCs effectively behave as a hard wall, despite being tuned to the characteristic time scale of the flow.

For all other values of the resistance ($R = 0.10$ and $R = 0.01$), the application of the IBCs results in a shortening of the near-wall streamwise turbulent integral length scales, exhibiting a well-defined periodic structure, noticeable especially in the autocorrelations $R_{vv}(\Delta x)$, $R_{pp}(\Delta x)$, and, less clearly, in $R_{uu}(\Delta x)$ and $R_{ww}(\Delta x)$. The strong periodic signature in R_{vv} and R_{pp} suggests the presence of predominantly wall-normal acoustic modes confined in the near-wall region. These occur exactly at the IBCs undamped resonant frequency, $\omega_r/2\pi$, as confirmed by one-point pressure time autocorrelations (not shown). The absence of a spanwise periodic structure suggest a purely streamwise propagation of the observed waves. No appreciable variation of the streamwise wavelength of such waves, λ_x, with y and the Mach number has been observed. The former suggests that the wave propagation speed is uniform in the newly established resonance layer, whereas the latter suggests, as expected, that the streamwise extent of the computational domain, L_x, constrains λ_x to be an integer fraction of L_x. Surprisingly, in all of the present calculations, $L_x/\lambda_x = 15$.

No trace of typical buffer layer streamwise and wall-normal vortical structures, responsible for sustaining the near-wall turbulence production cycle in the presence of a smooth wall (Jiménez & Pinelli 1999), is detected after the application of tuned IBCs. This is confirmed by near-wall ($y = -0.97$) spanwise autocorrelations of wall-normal velocity fluctuations, $R_{vv}(\Delta z)$, and streamwise velocity fluctuations, $R_{uu}(\Delta z)$, and by instantaneous visualizations showing a complete re-alignment of the coherent structures. Near-wall streaks are replaced entirely by spanwise elongated patterns of wall-normal and pressure fluctuations. The weaker periodic signature in $R_{uu}(\Delta x)$ and $R_{ww}(\Delta x)$ suggest that streamwise and spanwise velocity fluctuations do not play a dynamically relevant role in the sustainment of the observed periodic structures.

The streamwise wave propagation velocity, quantified by two-point temporal cross-correlations, differs from the local mean velocity. This suggests that the observed flow response cannot be explained by simply invoking inviscid Kelvin-Helmhotz instability mechanisms, as also found in the simulations by Jiménez *et al.* (2001) performed assuming incompressible flow and a purely real impedance at the wall. A rigorous stability analysis will be carried out in future work.

Although Jiménez *et al.* (2001) observed that rollers are primarily in the outer layer, modulating the near-wall streaks, in the present investigation (even for $\mathrm{M}_b = 0.05$ case), similar structures are present but remain confined near the wall. Moreover, while in the calculations of Jiménez *et al.* (2001), near-wall streaks are preserved even at the highest porosities investigated, in the present case smooth-wall turbulence production mechanisms are completely replaced by Kelvin-Helmholtz-like rollers. The observed spanwise rollers are connected by secondary streamwise vortical structures, consistent with mixing layer turbulence production dynamics (Figure 5).

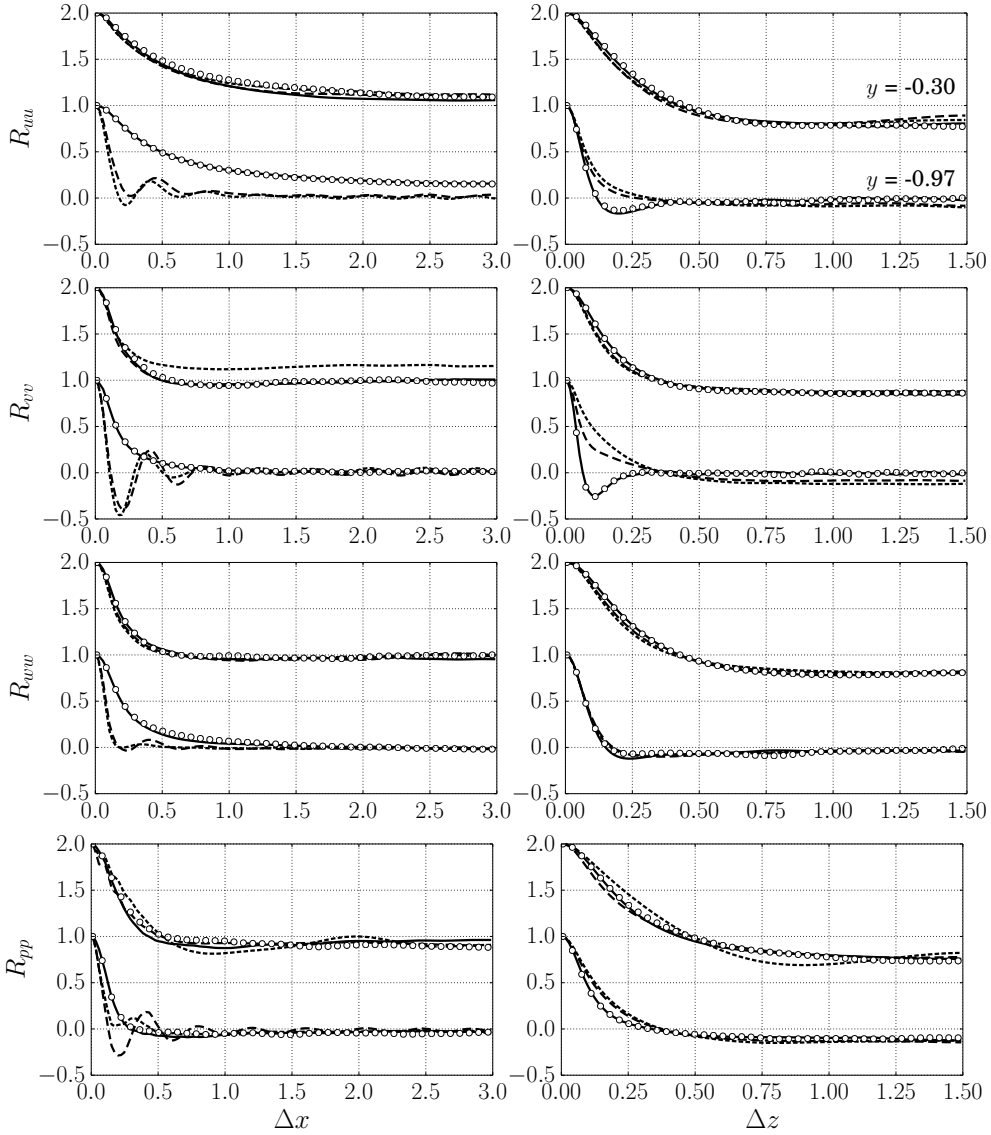

FIGURE 4. (left) Streamwise and (right) spanwise two-point autocorrelations for $M_b = 0.5$. Isothermal walls (no IBCs) (∘), with IBCs for $R = 1.00$ (—), $R = 0.10$ (– –) and $R = 0.01$ (- - -) for $\zeta = 0.5$, at y = -0.97 and y = -0.30 (shifted by +1).

4. Conclusions

We have investigated the possibility of passively controlling a compressible turbulent flow with the application of impedance boundary conditions (IBC). The latter are chosen as a three-parameter damped Helmholtz oscillator with undamped resonant frequency tuned, in all cases, to the characteristic time scale of the outer layer eddies, taken as the ratio of the bulk velocity over the boundary layer thickness. By also fixing the bulk Reynolds number to $Re_b = 6900$, the degrees of freedom of the overall dimensionless parameter space to explore are reduced to three: the bulk Mach number, M_b, the IBC's damping ratio, ζ, and resistance, R. A total of 27 large-eddy simulations (LES) have been

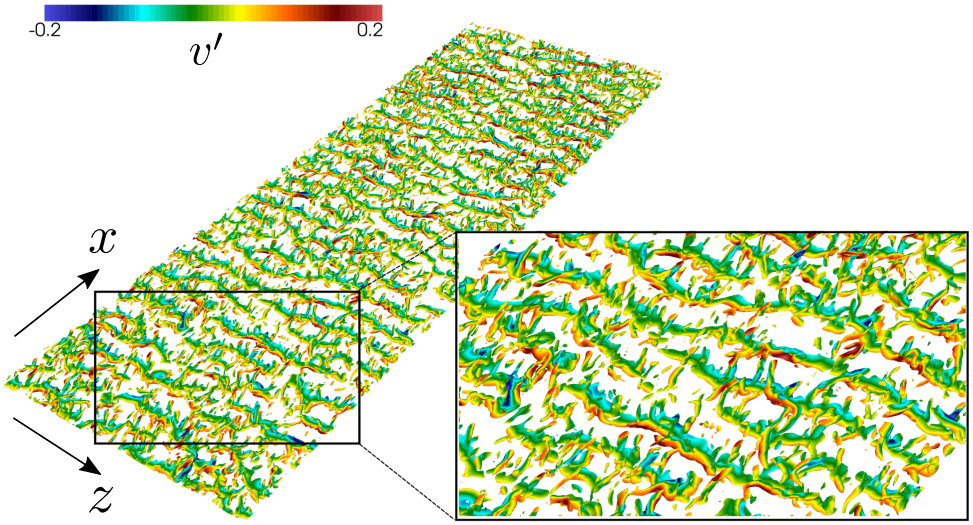

FIGURE 5. Iso-surfaces of second velocity gradient invariant $Q = 5.0$ for $1 + y < 0.90$ colored by vertical velocity fluctuations for $\mathrm{M}_b = 0.5$, $R = 0.01$, $\zeta = 0.5$

carried out to explore all possible combinations of three bulk Mach numbers ($\mathrm{M}_b = 0.05$, 0.2 , 0.5), three damping ratios ($\zeta = 0.5$, 0.7, 0.9), and three resistances ($R = 0.01$, 0.10, 1.00). Three additional LES with isothermal walls were performed at each Mach number to serve as reference simulations to estimate the drag increase. The IBCs have been formulated in the time domain by closely following Fung & Ju (2004) and coupled with a fully explicit compressible Navier-Stokes solver. Excellent agreement is observed between available semi-analytical solutions, assuming linear acoustics, and direct integration in time with a Navier-Stokes solver.

For sufficiently high Mach numbers, M_b, and low resistances, R, the application of tuned IBCs leads to a strong flow response, in the form of drag increase. The near-wall streaks disappear and are replaced by quasi periodic arrays of Kelvin-Helmholtz-like rollers. Time cross-correlations show that the propagating speed is the local convection velocity, confirming the hydrodynamic nature of the observed instability. The strong similarity between the near-wall spatial structure of wall-normal velocity and pressure fluctuation field suggests that wall-normal wave propagation in the near-wall region is driven (primarily) by acoustic energy exchange mechanisms occurring at the tuned frequency, $\omega_r = 2\,\pi\,\mathrm{M}_b$. The effects of the wave structure is evanescent in the outer layer. The alternation of the near-wall turbulent structure leads to a significant increase in the Reynolds shear stress near the wall. In particular the asymptotic value of Reynolds shear-stress gradient near the wall is non-zero, resulting in a departure of the mean velocity profiles from the law of the wall, while second order statistics normalized by friction velocity collapse at different R in the outer layer. This suggests that alterations to the turbulent flow structure remain confined near the wall in the first 15% of the boundary layer thickness.

Acknowledgments

Carlo Scalo thanks Prof. Dr. Jan Werner Delfs for the useful discussions (on an unrelated project) that have inspired the idea of tuning the impedance boundary conditions to the

characteristic time scales of the flow and Dr. Qiqi Wang for the discussions over the Mach number scaling of the drag increase. The computational resources were provided by CNRS on the BlueGene Q system Turing thanks to the GENCI-IDRIS Grant x20142a7178 as well as Purdue's supercomputer Conte.

REFERENCES

Bres, G. A., Inkman, M., Colonius, T. & Fedorov, A. V. 2013 Second-mode attenuation and cancellation by porous coatings in a high-speed boundary layer. *J. Fluid Mech.* **726**, 312 – 337.

Coleman, G. N., Kim, J. & Moser, R. D. 1995 A numerical study of turbulent supersonic isothermal-wall channel flow. *J. Fluid Mech.* **305**, 159–183.

Foysi, H., Sarkar, S. & Friedrich, R. 2004 Compressibility effects and turbulence scalings in supersonic channel flow. *J. Fluid Mech.* **509**, 207–216.

Fung, K. Y. & Ju, H. 2004 Time-domain Impedance Boundary Conditions for Computational Acoustics and Aeroacoustics. *Int. J. Comput. Fluid D.* **18**, 503–511.

Garcia-Mayoral, R. & Jiménez, J. 2011 Hydrodynamic stability and breakdown of the viscous regime over riblets. *J. Fluid Mech.* **678**, 317–347.

Ghosh, S., Foysi, H. & Friedrich, R. 2010 Compressible turbulent channel and pipe flow: similarities and differences. *J. Fluid Mech.* **648**, 155–181.

Ham, F., Mattsson, K., Iaccarino, G. & Moin, P. 2007 *Towards Time-Stable and Accurate LES on Unstructured Grids*, *Lecture Notes in Computational Science and Engineering*, vol. 56, pp. 235–249. Springer.

Huang, P. G., Coleman, G. N. & Bradshaw, P. 1995 Compressible turbulent channel flows: DNS results and modelling. *J. Fluid Mech.* **305**, 185–218.

Jiménez, J. & Pinelli, A. 1999 The autonomous cycle of near-wall turbulence. *J. Fluid Mech.* **389**, 335–359.

Jiménez, J., Uhlmann, M., Pinelli, A. & Kawahara, G. 2001 Turbulent shear flow over active and passive porous surfaces. *J. Fluid Mech.* **442**, 89–117.

Lechner, R., Sesterhenn, J. & Friedrich, R. 2001 Turbulent supersonic channel flow. *J. Turbul.* **2**, N1.

Ostoich, C., Bodony, D. J. & Geubelle, P. H. 2013 Interaction of a Mach 2.25 turbulent boundary layer with a fluttering panel using direct numerical simulation. *Phys. Fluids* **25**, 110806.

Shang, D. Y. & Wang, B. X. 1990 Effect of variable thermophysical properties on laminar free convection of gas. *Int. J. Heat Mass Transfer* **33**, 1387–1395.

Tam, C. K., Pastouchenko, N., Jones, M. G. & Watson, W. R. 2013 Experimental Validation of Numerical Simulation for An Acoustic Liner in Grazing Flow. *AIAA Paper 2013-2222.*

Tam, C. K. W. & Auriault, L. 1996 Time-domain Impedance Boundary Conditions for Computational Aeroacoustics. *AIAA J.* **34**, 917–923.

Vreman, A. W. 2004 An eddy-viscosity subgrid-scale model for turbulent shear flow: Algebraic theory and applications. *Phys. Fluids* **16**, 3670–3681.

Zhang, Q. & Bodony, D. J. 2012 Numerical investigation and modeling of acoustically-excited flow through a circular orifice backed by a hexagonal cavity. *J. Fluid Mech.* **693**, 367–401.